Acta Crystallographica Section D
Biological Crystallography
ISSN 0907-4449

Structure of the equine arteritis virus nucleocapsid protein reveals a dimer–dimer arrangement

Ashlesha Deshpande,[a] Sifang Wang,[a]‡ Martin A. Walsh[b] and Terje Dokland[a]*

[a]Department of Microbiology, University of Alabama at Birmingham, Birmingham, AL 35294, USA, and [b]MRC France, c/o European Synchrotron Radiation Facility, BP 220, 38043 Grenoble CEDEX, France

‡ Current address: Institute of Molecular and Cell Biology, Singapore.

Correspondence e-mail: dokland@uab.edu

Received 19 January 2007
Accepted 20 February 2007

PDB Reference: EAV N protein, 2i9f, r2i9fsf.

Equine arteritis virus (EAV) is an enveloped positive-sense RNA virus belonging to the *Arteriviridae* family, which also includes the porcine pathogen PRRSV and is genetically and structurally related to the coronaviruses. EAV is an important equine pathogen that has caused significant economic losses to the horse-breeding industry and has been difficult to control. The EAV virion consists of a genome-containing nucleocapsid core made of nucleocapsid (N) protein surrounded by a lipid envelope containing several membrane proteins. Here, the crystal structure of the capsid-forming domain of the EAV N protein is presented at 2.0 Å resolution. The dimeric N-protein structure is similar to the previously determined structure of the N protein from PRRSV, with most differences localized to the terminal helices and flexible loops. The N protein is organized as dimers of dimers in the crystal, which may reflect the arrangement of the protein in the viral nucleocapsid.

1. Introduction

The *Arteriviridae* is a family of enveloped positive-sense RNA viruses that includes two important agricultural pathogens, equine arteritis virus (EAV) and porcine reproductive and respiratory syndrome virus (PRRSV), in addition to lactate dehydrogenase-elevating virus (LDV) of mice and simian haemorrhagic fever virus (SHFV) (Plagemann, 1996; Snijder & Meulenberg, 1998). Arteriviruses are grouped together with coronaviruses in the order *Nidovirales* based on similarities in genome organization and expression (Cavanagh, 1997; Fauquet *et al.*, 2005; Snijder *et al.*, 1993).

EAV causes respiratory disease and reproductive failure in horses, mules and donkeys (Del Piero, 2000; MacLachlan & Balasuriya, 2006). The virus has increasingly become a problem to the $2 billion horse-breeding industry in the US and has proven difficult to control owing to its pattern of persistent subclinical infection with occasional outbreaks of the disease, in spite of the development of several effective vaccines (Balasuriya & MacLachlan, 2004). The related virus PRRSV is a major porcine pathogen in the US and infects pigs with a similar aetiology to EAV (Neumann *et al.*, 2005; Zimmerman *et al.*, 1997). Although the order *Nidovirales* includes important human pathogens such as the SARS coronavirus (SARS-CoV), there are no known human pathogens in the *Arteriviridae* family.

The EAV genome consists of a 12.7 kbp single-stranded positive-sense RNA that is transcribed as a set of subgenomic mRNA transcripts, each coding for a separate open reading frame (ORF; Snijder & Meulenberg, 1998). The first ORF encodes the nonstructural proteins, which include three or

Table 1
Crystallographic and refinement data.

Values in parentheses are for the highest resolution shell.

Data-collection statistics	
X-ray source	ESRF BM14
Wavelength (Å)	0.9781
Oscillation angle (°)	1.0
No. of frames	489
Resolution range (Å)	25.0–1.95 (2.06–1.95)
Total No. of reflections	498017
No. of unique reflections	25482
Completeness (%)	99.1 (98.2)
Redundancy	19.5 (19.2)
$R_{\rm merge}$†	0.079 (0.525)
$I/\sigma(I)$	8.4 (1.5)
Refinement parameters	
Resolution range (Å)	25.0–2.0 (2.05–2.0)
No. of reflections	22474 (1609)
No. of atoms	2075
$R_{\rm cryst}$‡	0.219
$R_{\rm free}$‡	0.248
R.m.s.d. on bond lengths (Å)	0.018
R.m.s.d. on bond angles (°)	1.623
Ramachandran statistics, residues in (%)	
Most favoured region	91.3
Allowed region	8.2
Generously allowed region	1.0
Disallowed region	0.0

† $R_{\rm merge} = \sum_h \sum_i |I_{h,i} - \langle I_h \rangle| / \sum_h \sum_i I_{h,i}$. ‡ $R_{\rm cryst} = \sum_h |F_{{\rm obs},h} - F_{{\rm calc},h}| / \sum_h |F_{{\rm obs},h}|$. $R_{\rm free}$ is the same but calculated for a random 5% of reflections not used in refinement.

four proteases, an RNA-dependent RNA polymerase, a helicase and an endonuclease, while ORFs 2–5 encode glycosylated membrane proteins (GP2, E and GP3–GP5), ORF6 encodes the nonglycosylated membrane (M) protein and ORF7 encodes the nucleocapsid (N) protein (Snijder & Meulenberg, 1998; Wieringa *et al.*, 2004). In electron micrographs arterivirus virions appear as smooth roughly spherical or oblong particles with a diameter of about 60 nm (Horzinek, 1981; Snijder & Meulenberg, 1998; Wieringa *et al.*, 2004). The major components of the envelope are GP5 and M, which form disulfide-linked heterodimers and are essential for virion assembly (Snijder *et al.*, 2003; Wieringa *et al.*, 2004). GP5 may also be involved in receptor binding, but the minor envelope proteins are essential for infectivity and may be the main determinants for tropism (Dobbe *et al.*, 2001). Replication and assembly occur at internal membranes and are probably driven by interactions between N and the envelope proteins (Snijder & Meulenberg, 1998).

The N protein of EAV (EAV-N) consists of 110 residues, while that of PRRSV contains 123 residues, with several additional amino acids in the N-terminal half of the protein (Fig. 1). The amino-terminal half of EAV-N (1–47) is the least conserved part of the sequence; it contains a number of positively charged residues and is involved in RNA binding. The arterivirus N protein is targeted to the nucleus of infected cells, suggesting that N is involved in the modulation of host functions in addition to its role in RNA packaging and assembly (Tijms *et al.*, 2002; Yoo *et al.*, 2003).

We previously determined the structure of the C-terminal half (residues 58–123) of the PRRSV N protein (PRRSV-NΔ57), which forms a dimer that is considered to comprise the capsid-forming domain of N (Doan & Dokland, 2003*b*). Here, we present the structure of the equivalent domain of EAV-N (residues 49–110). In both viruses, the protein forms a tight dimer consisting of a β-sheet that is capped and flanked by α-helices. However, in EAV the N protein forms a dimer of dimers in the crystal, which may reflect the arrangement of the protein in the viral nucleocapsid.

2. Methods

2.1. Cloning, expression, purification and crystallization

Residues 49–110 of EAV-N were cloned into the vector pET16b, incorporating an N-terminal His_6 tag (MAHH-HHHH . . .) immediately preceding the EAV-N sequence, and expressed in *Escherichia coli* BL21(DE3) as previously described for PRRSV-NΔ57 (Doan & Dokland, 2003*a*). To obtain SeMet-derivative crystals, the clones were grown for 15 h at 310 K in M9 media supplemented with glucose, all amino acids except Met, vitamins and SeMet (Gerchman *et al.*, 1994). After lysis by passage through an Avestin Emulsiflex EF-C3 high-pressure disruptor, the protein was purified by affinity on a Hi-Trap Ni-chelating column (Amersham Bio-

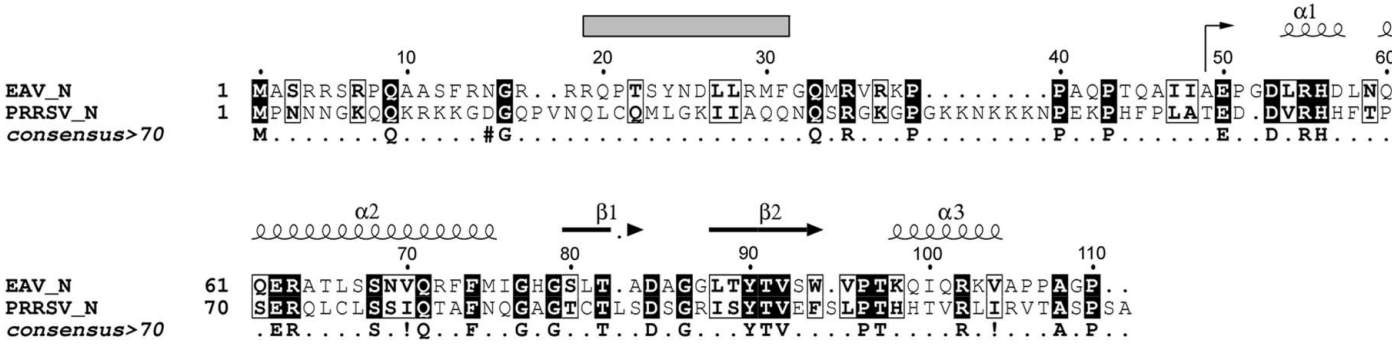

Figure 1
Sequence alignment of EAV-N and PRRSV-N. The alignment was performed with *ClustalW* (Chenna *et al.*, 2003) and numbered according to EAV-N. Identical residues are shown in black boxes; similar residues are shown in white boxes. The arrow at residue 49 indicates the start of the EAV-NΔ48 construct used in our study. Secondary-structure elements of the EAV-NΔ48 structure are shown above the sequence. The grey box above residues 19–31 indicates a predicted α-helix. This figure was created with *ESPript* (Gouet *et al.*, 1999).

sciences) followed by size-exclusion chromatography on Sephacryl S-200 (Amersham Biosciences). The protein was concentrated to 30 mg ml^{-1} and crystallized by vapour diffusion against 0.1 *M* sodium phosphate pH 8.0 and 25% PEG 3350 for 8 d at 291 K. The crystals were harvested, briefly soaked in 10% glycerol, 0.15 *M* sodium phosphate pH 8.0 and 27% PEG 3350 and frozen by immersion in liquid nitrogen.

2.2. Data collection and structure determination

Data were collected at the UK beamline BM14 at the ESRF using a single frozen crystal that was auto-mounted onto the BM14 beamline goniometer using the SC3 robotic sample changer (Cipriani *et al.*, 2006). An X-ray fluorescence scan was performed to ascertain the Se edge and anomalous scattering factors were calculated using the program *CHOOCH* (Evans & Pettifer, 2001). A total of 489 frames of data were collected on a MAR Mosaic 225 CCD area detector at the experimentally determined selenium absorption-edge peak energy (12.67587 keV, 0.9781 Å) with an oscillation angle of 1.0°. The data were integrated and scaled using the programs *XDS* (Kabsch, 1993) and *SCALA* (Collaborative Computational Project, Number 4, 1994), giving a data set with a redundancy of 19.5 and an overall $R_{\rm merge}$ of 7.9% (Table 1). The crystals belonged to space group $C222_1$, with unit-cell parameters $a = 68.23$, $b = 73.23$, $c = 138.60$ Å, corresponding to two dimers in the asymmetric unit with $V_{\rm M} = 2.78$ Å^3 Da^{-1}. The selenomethionine-derivative crystals showed a high degree of mosaicity (>2°), with usable data extending to about 2.0 Å resolution. Initial phasing was performed with *SHELXE* (Sheldrick, 2002) followed by fourfold noncrystallographic symmetry averaging, and solvent flattening was performed using *DM* (Cowtan & Main, 1998). The resulting map could be readily interpreted by comparison with the PRRSV-NΔ57 structure and most of the *A*, *B*, *C* and *D* subunits were built automatically using *ARP*/*wARP* (Morris *et al.*, 2003). Further model building was performed with *O* (Jones *et al.*, 1991) and refinement was performed using *REFMAC* (Murshudov *et al.*, 1997). Initial rounds of refinement used NCS restraints, which were relaxed in the final rounds. The final model has $R_{\rm cryst} = 0.219$ and $R_{\rm free} = 0.248$ (Table 1).

3. Results and discussion

3.1. Structure determination

EAV-NΔ48, comprising residues 49–110 of EAV-N (Fig. 1), was cloned and expressed in *E. coli* with an N-terminal His_6 tag, purified by nickel-affinity and size-exclusion chromatography and crystallized by the hanging-drop vapour diffusion against 0.1 *M* sodium phosphate pH 8.0 and 25% polyethylene glycol (PEG) 3350. The crystals belong to the orthorhombic space group $C222_1$, with unit-cell parameters $a = 68.23$, $b = 73.23$, $c = 138.60$ Å, and diffracted X-rays to beyond 2 Å resolution at the UK CRG beamline BM14 at the ESRF (Table 1). The EAV-NΔ48 structure was solved to a resolution of 2.0 Å by single-wavelength anomalous diffraction (SAD) phasing on an SeMet derivative. The resulting model (Fig. 2) was refined with *REFMAC* against these data to a final $R_{\rm cryst}$ of 21.9% and $R_{\rm free}$ of 24.8%.

3.2. Structure of EAV-N

EAV-NΔ48 forms a dimer with a similar structure to that of the previously solved PRRSV-NΔ57 structure (Doan & Dokland, 2003*b*), consisting of a four-stranded antiparallel β-sheet capped by two long α-helices (α2) and flanked by shorter N- and C-terminal helices (Figs. 2*b* and 3*a*). Two such dimers are arranged around a noncrystallographic twofold axis into a dimer of dimers that comprises the crystal asymmetric unit (Fig. 3*a*). Interactions between the two dimers are mediated by ten water molecules that occupy the space between strand β2 of subunits *A* and *C* (Fig. 3*a*). This water

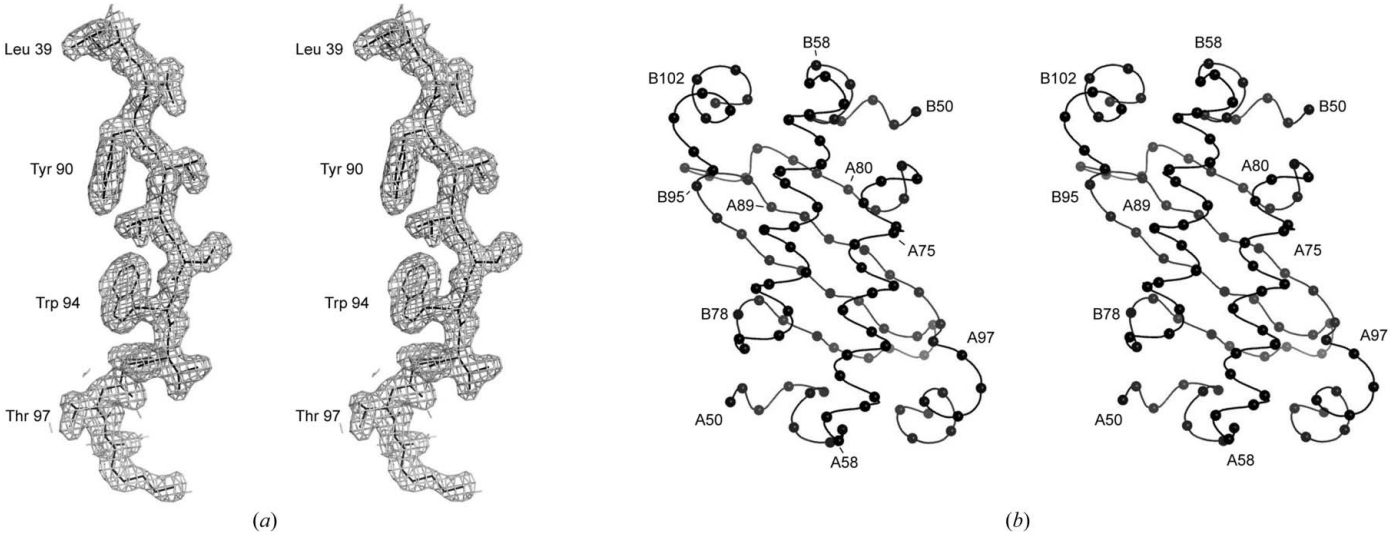

Figure 2
Structure of EAV-NΔ48. (*a*) Stereo diagram of representative electron density from the final $2F_{\rm o} - F_{\rm c}$ map, showing residues Leu88–Lys49 in the β2 strand. (*b*) Stereo diagram of the C^{α} backbone of the *AB* dimer structure. Pertinent residues are labelled for orientation.

hole displays a strongly positively charged surface on the α-helical side of the tetramer (Fig. 4*a*). In contrast, the surface of the β-sheet floor has an overall negative charge (Fig. 4*b*). The structure also showed the N-terminal His_6 tag for subunits *A*, *B* and *D*, but the last five residues of the C-terminus (PPAGP) were disordered in all four subunits.

The four subunits making up the two dimers in the asymmetric unit are very similar and could be superimposed with pairwise root-mean-square deviations (r.m.s.d.s) ranging from 0.3 to 0.7 Å (Fig. 3*b*). Likewise, the *AB* dimer could be superimposed on the *CD* dimer with an r.m.s.d. of 0.7 Å. Nevertheless, there is some variation, primarily localized to residues Ala83–Gly86 which form the loop between β-strands $\beta1$ and $\beta2$ (the 'β-loop'), and to a lesser extent in the N- and C-terminal α-helices (Fig. 3*b*). Indeed, the electron density for the β-loop was poor in subunits *A* and *D*, presumably reflecting their exposed location on the outside of the tetramer. Such variation could potentially reflect the conformational variability required for the assembly of an icosahedral shell with more than 60 subunits (Caspar & Klug, 1962; Dokland, 2000).

The flexibility in the subunits is also reflected in the *B* factors. The greatest mobility is found in the C-terminal helix $\alpha3$, as well as in the variable β-loop (Fig. 3*c*). However, there are clear differences in the degree of mobility in the four subunits. Overall, subunit *D* is far more mobile than the other three. The *B* factor in $\alpha3$ of subunit *D* is as high as 72.2 $Å^2$, compared with a mean *B* factor of 32.2 $Å^2$ for the whole structure. In addition, there is a flexible region in the part of subunit *C* that forms the outer surface of the tetramer. This mobility is a consequence of the lack of contacts between the *CD* dimer and the symmetry-related *CD* at this end of the tetramer. In contrast, the *AB* dimer, which forms strong contacts with the symmetry-related *AB* dimer across the crystal twofold axis at this end of the molecule (see below), displays much lower mobility at the equivalent molecular interface (Fig. 3*c*).

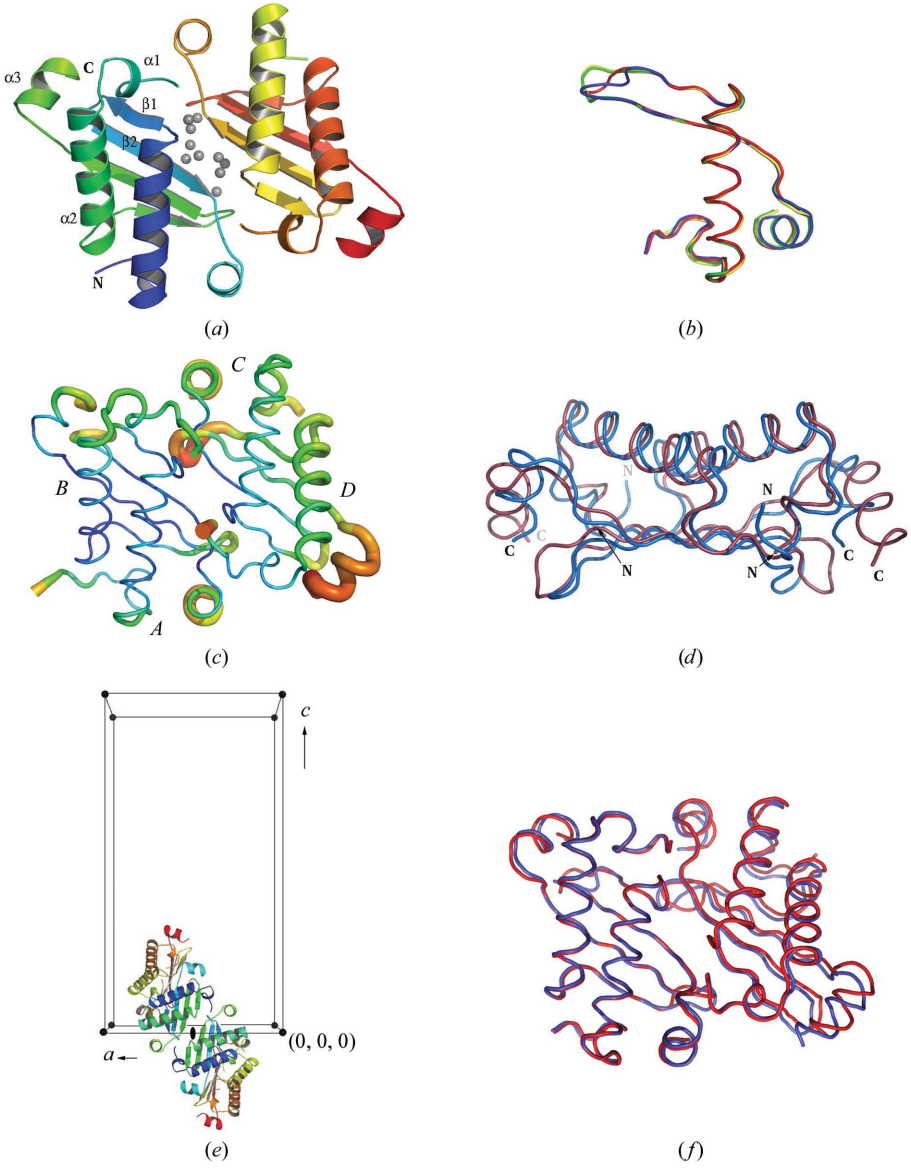

Figure 3
The EAV-NΔ48 structure. (*a*) Ribbon representation of the two dimers in the asymmetric unit, coloured in a spectrum from blue (subunit *A*) through green (subunit *B*) and yellow (subunit *C*) to red (subunit *D*). The ten water molecules between the *AB* and *CD* dimers are shown as grey spheres. Secondary-structure elements in the *A* and *B* subunits are labelled. (*b*) Superposition of the C^α backbones of all four subunits, coloured as in (*a*). (*c*) Worm trace of the *AB*–*CD* tetramer backbone. The tube thickness and colour reflect the average residue *B* factors (thin/blue, low; thick/red, high). (*d*) Superposition of the C^α backbones of the EAV-N *AB* dimer (blue) on the PRRSV-N dimer (red). N- and C-termini are indicated. (*e*) Ribbon representation of the *AB*–*CD* tetramer and the *A*′*B*′–*C*′*D*′ tetramer related to *AB*–*CD* by the crystallographic twofold symmetry axis parallel to *b* in the *ab* plane (filled oval). The unit cell is indicated with balls at each corner. (*f*) Superposition of the *AB*–*CD* tetramer (blue) with the *AB*–*A*′*B*′ tetramer (red). (For this experiment, only one of the two dimers in the each tetramer was superimposed in order to emphasize the difference in angle between the two tetramers.) All figures were produced using *PyMOL* (DeLano, 2002).

3.3. Comparison with other nidoviral nucleocapsid proteins

The N protein in EAV consists of 110 residues, compared with 123 residues in PRRSV (Fig. 1). The largest sequence difference between the EAV and PRRSV N proteins exists in the N-terminal RNA-binding domain, in which there are ten fewer residues in EAV-N and the sequence identity is less than 16%. Notably, many of the positively charged Lys residues involved in RNA binding and the Cys residues considered important for assembly in PRRSV (Wootton & Yoo, 2003) are absent in EAV.

In contrast, the C-terminal capsid-forming domains represented by the present structure share about 35% sequence identity. The greatest sequence divergence is in the α2 helix, which is exposed on the outer surface of the protein. These residues are presumed to form virus-specific interactions with other viral proteins and do not directly affect the three-dimensional conformation of the N protein. Consequently, the two structures are very similar, with an overall r.m.s.d. of 2.6 Å for the *A* subunit. The largest difference is found in the C-terminal helix α3 and in the β-loop, which are 3.9 and 4.0 Å apart, respectively, in the *A* subunits of EAV-N and PRRSV-N. These also correspond to the regions of highest flexibility in EAV-N. The r.m.s.d. between EAV-N and PRRSV-N increases to 2.8 Å when the whole dimer is considered, indicating that there are additional differences between EAV-N and PRRSV-N in the way the monomers are organized into a dimer; EAV-N forms a tighter dimer than PRRSV-N (Fig. 3*d*).

Coronaviruses have much larger nucleocapsid proteins than arteriviruses: up to 422 residues in the case of SARS-CoV. An arterivirus-like nucleocapsid domain was recently discovered in the C-terminal dimerization domains of the nucleocapsid proteins from the coronaviruses IBV and SARS-CoV (Chang *et al.*, 2005; Jayaram *et al.*, 2006; Yu *et al.*, 2006). In these structures, the orientation of the α-helices relative to the β-sheet differs from that in EAV and PRRSV, but the topology is the same and could be classified as the 'nidoviral nucleocapsid fold'. Thus, the evolutionary relationships between arteriviruses and coronaviruses evidenced by the similar organization of the genomes is also reflected in the nucleocapsid protein structures and will probably also be reflected in other viral protein structures. The nidoviral nucleocapsid fold differs from the nucleocapsid proteins of both the flaviviruses (Dokland *et al.*, 2004) and the alphaviruses (Choi *et al.*, 1997).

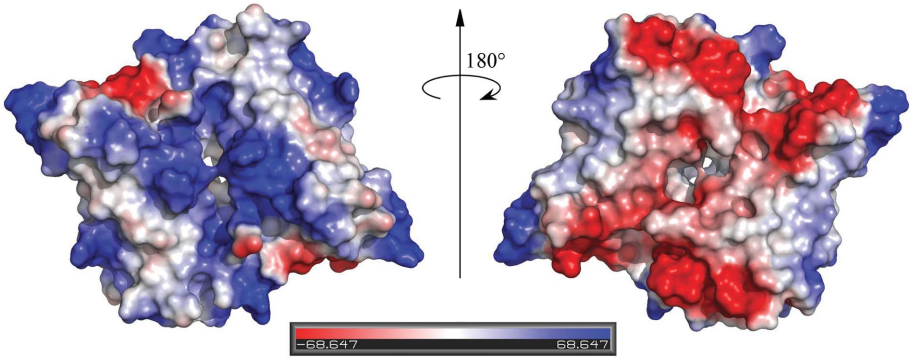

Figure 4
Electrostatic potential surface of the EAV-NΔ48 *AB–CD* tetramer. (*a*) Viewed in the same orientation as Fig. 2(*a*), looking down at the α2 helices. (*b*) Looking down at the β-sheets after turning the tetramer 180° around *y*. This figure was produced using *PyMOL* (DeLano, 2002).

3.4. Assembly and structure of the virion

As previously pointed out, the arterivirus N protein resembles the coat protein of RNA bacteriophage MS2, although the MS2 protein has a wider eight-stranded β-sheet and α-helices in a different orientation (Doan & Dokland, 2003*b*; Valegård *et al.*, 1990). The organization of MS2 thus provides a reasonable starting point for under-

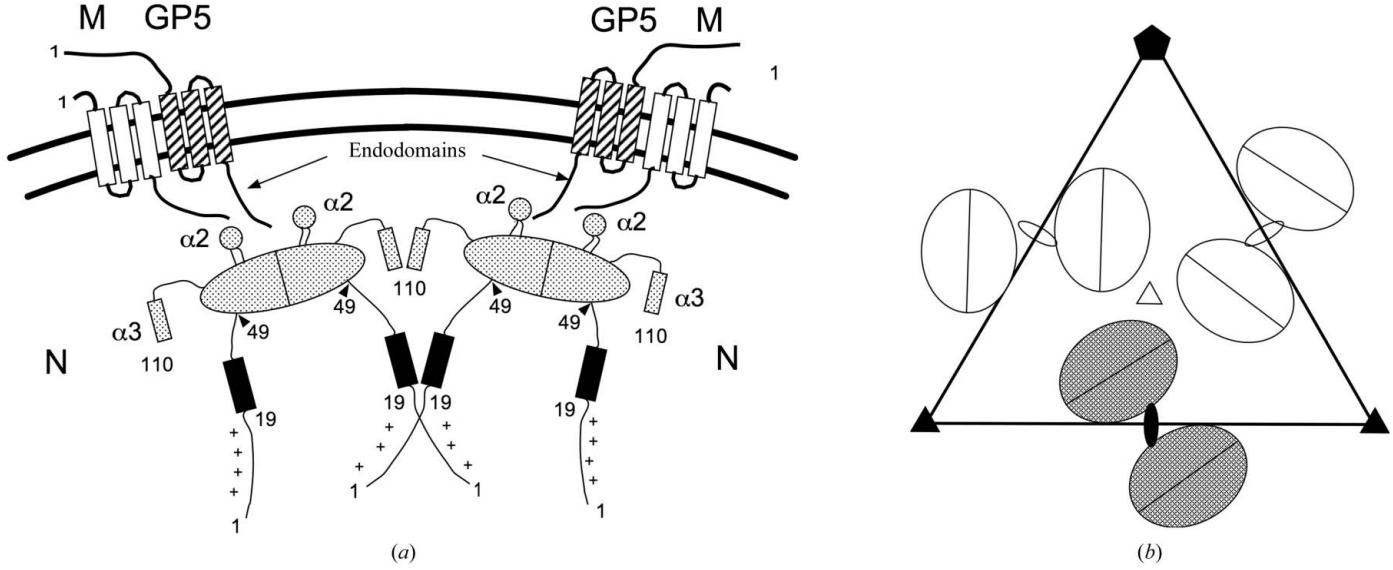

Figure 5
Model for the arrangement of N in the EAV virion. (*a*) Schematic diagram of the organization and protein–protein interactions of protein N. The three transmembrane domains of the major envelope proteins M and GP5 are shown as open and hatched boxes, respectively. The N dimers are represented by dotted ovals, with the flanking α2 and α3 helices indicated. The predicted α-helix in the N-terminal domain is shown in black. (*b*) Schematic diagram of the possible arrangement of EAV-N dimers (ovals) in the nucleocapsid shell. One icosahedral asymmetric unit triangle is shown; icosahedral symmetry elements are indicated with black symbols, while quasi-symmetry elements are shown as open symbols.

standing the organization of N in the EAV nucleocapsid. In this model, the β-sheet of the dimer would face the inside of the shell, where the N-terminal domains would be positioned to interact with the RNA (Fig. 5*a*). The α-helical outer surface might form a docking site for the envelope proteins, most likely the endodomains of the major envelope proteins M and/or GP5 (Fig. 5*a*; Doan & Dokland, 2003*b*). Assembly of the shell is probably mediated through interactions between the predicted α-helix in residues 19–31 as well as with the RNA.

In order to build an icosahedral shell with more than 60 subunits (or any nonsymmetric large shell) there has to be some conformational variability and/or differences in subunit interactions between the capsid-protein subunits (Caspar & Klug, 1962; Dokland, 2000). In the $T = 3$ plant viruses, for example, such conformational variation is generated through the formation of two different types of dimers: a flat *CD* dimer and a curved *AB* dimer (Abad-Zapatero *et al.*, 1980; Harrison *et al.*, 1978). The differences in dimer organization are reflected in conformational differences and order–disorder transitions in the N-terminal part of the protein.

In the EAV-N crystal structure, the two dimers (*AB* and *CD*) that comprise the tetramer in the crystal asymmetric unit are organized *via* a quasi-twofold axis so that the β-sheets of both dimers are more or less facing the same way (Fig. 3*a*). This tetramer is almost identical to that formed by the *AB* dimer and the $A'B'$ dimer related by the crystallographic twofold axis (Figs. 3*e* and 3*f*). It is tempting to suggest that the tetramer comprises the building block for the shell and that the quasi-equivalence between these two types of tetramers reflects the organization of the N protein in the virus. For example, we might build a shell with a diameter of around 31–38 nm from 360 copies of N (Fig. 5*b*). However, there is currently no experimental evidence to support this model and crystal contacts are not necessarily an indicator of *in vivo* interactions. Confirmation of this model would have to await characterization of the arterivirus structure by cryo-electron microscopy and three-dimensional reconstruction.

We are grateful to Dr Eric Snijder at Leiden University for suggesting this project, for providing us with the original EAV-N clone and for his continued support of this work.

References

Abad-Zapatero, C., Abdel-Meguid, S. S., Johnson, J. E., Leslie, A. G. W., Rayment, I., Rossmann, M. G., Suck, D. & Tsukihara, T. (1980). *Nature (London)*, **286**, 33–39.

Balasuriya, U. B. & MacLachlan, N. J. (2004). *Vet. Immunol. Immunopathol.* **102**, 107–129.

Caspar, D. L. D. & Klug, A. (1962). *Cold Spring Harbor Symp. Quant. Biol.* **27**, 1–24.

Cavanagh, D. (1997). *Arch. Virol.* **142**, 629–633.

Chang, C. K., Sue, S. C., Yu, T. H., Hsieh, C. M., Tsai, C. K., Chiang, Y. C., Lee, S. J., Hsiao, H. H., Wu, W. J., Chang, C. F. & Huang, T. H. (2005). *FEBS Lett.* **579**, 5563–5668.

Chenna, R., Sugawara, H., Koike, T., Lopez, R., Gibson, T. J., Higgins, D. G. & Thompson, J. D. (2003). *Nucleic Acids Res.* **31**, 3497–3500.

Choi, H. K., Lu, G., Lee, S., Wengler, G. & Rossmann, M. G. (1997). *Proteins*, **27**, 345–359.

Cipriani, F. *et al.* (2006). *Acta Cryst.* D**62**, 1251–1259.

Collaborative Computational Project, Number 4 (1994). *Acta Cryst.* D**50**, 760–763.

Cowtan, K. & Main, P. (1998). *Acta Cryst.* D**54**, 487–493.

Del Piero, F. (2000). *Vet. Pathol.* **37**, 287–296.

DeLano, W. L. (2002). *The PyMOL Molecular Graphics System.* San Carlos, CA, USA: DeLano Scientific.

Doan, D. & Dokland, T. (2003*a*). *Acta Cryst.* D**59**, 1504–1506.

Doan, D. & Dokland, T. (2003*b*). *Structure*, **11**, 1445–1451.

Dobbe, J. C., van der Meer, Y., Spaan, W. J. M. & Snijder, E. J. (2001). *Virology*, **286**, 283–294.

Dokland, T. (2000). *Structure*, **8**, R157–R167.

Dokland, T., Walsh, M., MacKenzie, J. M., Khromykh, A. A., Ee, K.-H. & Wang, S. (2004). *Structure*, **12**, 1157–1163.

Evans, G. & Pettifer, R. F. (2001). *J. Appl. Cryst.* **34**, 82–86.

Fauquet, C. M., Mayo, M. A., Maniloff, J., Desselberger, U. & Ball, L. A. (2005). Editors. *Virus Taxonomy: VIIIth Report of the International Committee on Taxonomy of Viruses.* San Diego: Elsevier/Academic Press.

Gerchman, S. E., Graziano, V. & Ramakrishnan, V. (1994). *Protein Expr. Purif.* **5**, 242–251.

Gouet, P., Courcelle, E., Stuart, D. I. & Metoz, F. (1999). *Bioinformatics*, **15**, 305–308.

Harrison, S. C., Olson, A. J., Schutt, C. E., Winkler, F. K. & Bricogne, G. (1978). *Nature (London)*, **276**, 368–373.

Horzinek, M. C. (1981). *Non-arthropod-borne Togaviruses.* London: Academic Press.

Jayaram, H., Fan, H., Bowman, B. R., Ooi, A., Jayaram, J., Collisson, E. W., Lescar, J. & Prasad, B. V. V. (2006). *J. Virol.* **80**, 6612–6620.

Jones, T. A., Zou, J.-Y., Cowan, S. W. & Kjeldgaard, M. (1991). *Acta Cryst.* A**47**, 110–119.

Kabsch, W. J. (1993). *J. Appl. Cryst.* **26**, 795–800.

MacLachlan, N. J. & Balasuriya, U. B. (2006). *Adv. Exp. Med. Biol.* **581**, 429–433.

Morris, R. J., Perrakis, A. & Lamzin, V. S. (2003). *Methods Enzymol.* **374**, 229–244.

Murshudov, G. N., Vagin, A. A. & Dodson, E. J. (1997). *Acta Cryst.* D**53**, 240–255.

Neumann, E. J., Kliebenstein, J. B., Johnson, C. D., Mabry, J. W., Bush, E. J., Seitzinger, A. H., Green, A. L. & Zimmerman, J. J. (2005). *J. Am. Vet. Med. Assoc.* **3**, 385–392.

Plagemann, P. G. W. (1996). *Fields Virology*, 3rd ed., edited by B. N. Fields, D. M. Knipe & P. M. Howley, pp. 1105–1120. Philadelphia: Lippincott–Raven.

Sheldrick, G. M. (2002). *Z. Kristallogr.* **217**, 644–650.

Snijder, E. J., Dobbe, J. C. & Spaan, W. J. M. (2003). *J. Virol.* **77**, 97–104.

Snijder, E. J., Horzinek, M. C. & Spaan, W. J. M. (1993). *Adv. Exp. Med. Biol.* **342**, 235–244.

Snijder, E. J. & Meulenberg, J. J. M. (1998). *J. Gen. Virol.* **79**, 961–979.

Tijms, M. A., van der Meer, Y. & Snijder, E. J. (2002). *J. Gen. Virol.* **83**, 795–800.

Valegård, K., Liljas, L., Fridborg, K. & Unge, T. (1990). *Nature (London)*, **345**, 36–41.

Wieringa, R., de Vries, A. A., van der Meulen, J., Godeke, G. J., Onderwater, J. J., van Tol, H., Koerten, H. K., Mommaas, A. M., Snijder, E. J. & Rottier, P. J. M. (2004). *J. Virol.* **78**, 13019–13027.

Wootton, S. & Yoo, D. (2003). *J. Virol.* **77**, 4546–4557.

Yoo, D., Wootton, S., Li, G., Song, S. & Rowland, R. R. (2003). *J. Virol.* **77**, 12173–12183.

Yu, I. M., Oldham, M. L., Zhang, J. & Chen, J. (2006). *J. Biol. Chem.* **281**, 17134–17139.

Zimmerman, J. J., Yoon, K. J., Wills, R. W. & Swenson, S. L. (1997). *Vet. Microbiol.* **55**, 187–196.